Influence of load history on the force-displacement response of in-plane loaded unreinforced masonry walls

Bastian Valentin Wilding[1]

bastian.wilding@epfl.ch

Kiarash Dolatshahi[1,2]

dolatshahi@sharif.edu

Katrin Beyer[1] – corresponding author

katrin.beyer@epfl.ch

[1]Earthquake Engineering and Structural Dynamics Laboratory (EESD), School of Architecture, Civil and Environmental Engineering (ENAC), École Polytechnique Fédérale de Lausanne (EPFL), EPFL ENAC IIC EESD, GC B2 504, Station 18, 1015 Lausanne, Switzerland

[2]Department of Civil Engineering, Sharif University of Technology, Room 515, Tehran, Iran

Abstract

Empirical drift capacity models for in-plane loaded unreinforced masonry (URM) walls are derived from results of quasi-static cyclic tests. The experimentally determined drift capacities are, however, dependent on the applied demand, i.e., on the loading protocol that is used in the test. These loading protocols differ between test campaigns. The loading protocols applied in tests are also different from the displacement histories to which URM walls are subjected in real earthquakes. In the absence of experimental studies on the effect of loading histories on the wall response, this article presents numerical simulations of modern unreinforced clay block masonry walls that are subjected to different loading protocols. The study shows that the force capacity is not very sensitive to the loading protocol. The drift capacity of walls failing in shear is, however, rather sensitive to the loading protocol while the drift capacity of walls failing in flexure is not as sensitive. The largest difference in drift capacity of up to 100 % is observed between monotonic and cyclic loading for shear controlled walls under double fixed boundary conditions and low axial load ratios.

1   Introduction

Displacement-based seismic assessment of unreinforced masonry (URM) buildings requires as input—among other parameters—the nonlinear force-displacement response of the in-plane loaded URM walls. The latter is often approximated by a bilinear curve, which is described by the effective stiffness, the peak shear strength and the drift capacity of the wall, drift being the horizontal displacement divided by the wall height. In many codes [1–4], drift capacities are determined with empirical models that have been fitted to data of quasi-static cyclic shear-compression tests of URM walls. Yet, the drift capacities of URM walls seem to depend on the load history to which the walls are subjected to during the test. To the author's knowledge, the only pairs of URM walls tested using different loading protocols (monotonic vs. reversed-cyclic) stem from campaigns by Ganz & Thürlimann [5] and Magenes & Calvi [6]. As mentioned in [7], the cyclic tests led to a slightly greater effective stiffness and a slightly smaller shear force capacity when compared to the monotonic tests. The most significant effect was observed for the drift capacity, for which the one obtained from the cyclic test was only about half that from the monotonic test.

In a test campaign on reinforced masonry walls by Tomazevic et al. [8] multiple identical specimens were subjected to different loading protocols: monotonic loading, reversed-cyclic loading and reversed-cyclic loading superimposed with an additional sine function as well as a load history corresponding to a simulated earthquake. While the two cyclic loading protocols led to similar force and drift capacities as the simulated earthquake, the shear force and drift capacities obtained from the monotonic tests were significantly greater. Therefore, the loading protocol used in quasi-static cyclic tests appears to influence the outcome of those tests [9,10]. However, loading protocols differ between test campaigns (e.g. [5,11–14]). The most common loading protocols comprise cycles of zero mean with increasing amplitudes but both the applied drift limits and the number of cycles per drift limit vary; examples of loading protocols are given in [10,15–23]. Moreover, the loading caused by a real seismic event might be rather different from the loading histories applied in laboratory tests.

The cumulative drifts $\Sigma abs(\delta_i)$ up to a reference drift capacity of 1% that result from loading protocols designed for test campaigns on full-scale masonry walls loaded in-plane are compared in Figure 1a. The plot shows that the cumulative drifts of the various protocols differ by as much as a factor of four. All loading protocols that

were effectively used in test campaigns on masonry walls (B04, B06, PB15, S15) imposed a higher cumulative demand than the loading protocols that were derived to represent the demand in regions of low to moderate seismicity (protocol MBL by Mergos & Beyer [10]). As a result, the drift capacity obtained from these tests might be smaller than that of a corresponding wall when subjected to the demand of a design level earthquake from a region of low to moderate seismicity. Note that the protocols MBL and MBH depend on the fundamental period T of the structure and yield therefore a range of values as T was assumed to vary between 0.1 and ≥ 0.5 s.
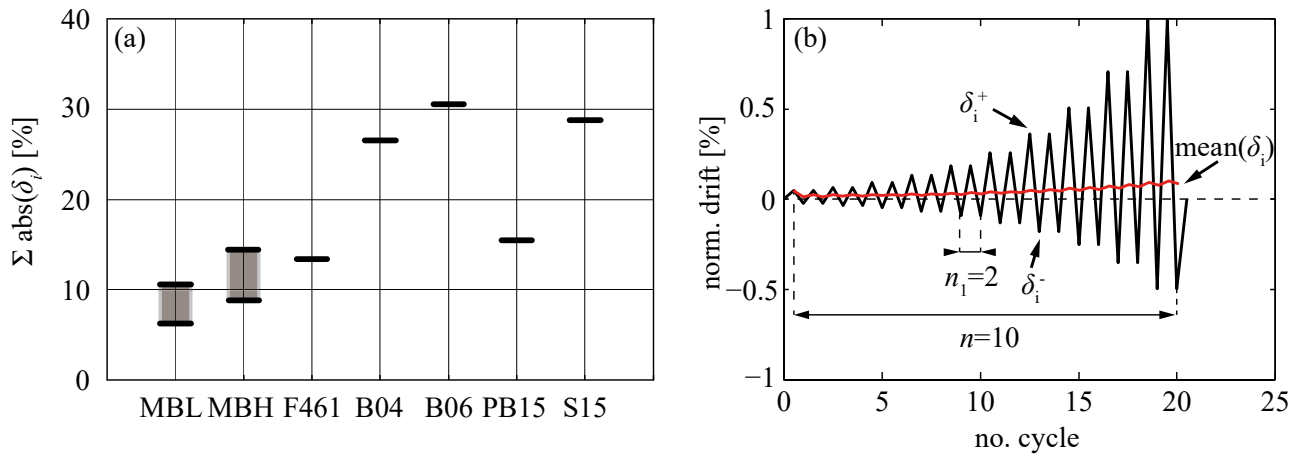

Figure 1: (a) comparison of the cumulative drift up to a reference drift capacity of 1 % (MBL – Mergos & Beyer [10] full range of considered periods of structures for regions of low to moderate seismicity, MBH – Mergos & Beyer [10] full range of considered periods of structures for high seismicity regions, F461 – FEMA461 [22], B04 – protocol used in test campaign by [11], B06 – protocol used in test campaign by [12], PB15 – protocol used in test campaign by [14], S15 – protocol used in test campaign by [13]; (b) loading protocol with non-zero mean of drift limits introducing number of drift limits n, number of cycles per drift limit n_1 and drift limit mean

The load histories to which URM walls are subjected during real earthquakes or laboratory tests might differ with regard to (i) the applied drift limits δ_i, (ii) the sequence of those drift limits, (iii) the number n_1 of cycles per drift limit and (iv) the mean of the drift cycles (Figure 1b). This paper investigates through numerical studies the influence of these parameters on the force-displacement response of URM walls. The effect of the strain rate on the force-displacement response, which is a further parameter that differs between typical laboratory and real loading conditions, is not investigated here.

In the following, a numerical study is carried out simulating quasi-static cyclic tests on URM walls for different loading protocols. The numerical model is explained and validated in Section 2. In Sections 3 to 4, the

parametric study is outlined and the results are presented, interpreted and conclusions on the effect of the load history on the URM wall response are drawn. A first simple model that accounts for load history effects on the drift capacity of walls failing in shear is proposed in Section 5.

2   **Analysis procedure**

A numerical study is performed to assess the influence of the load history on stiffness, strength and deformation capacity of URM walls. The simulated walls are modern clay block masonry walls with joints of normal thickness (~1 cm), which have been tested with one loading protocol experimentally. First, the wall configurations are presented, which correspond to wall configurations that have been tested experimentally for a reversed-cyclic loading protocol. Second, the numerical modeling approach, the material laws and parameters are introduced. Finally, the numerical model is validated against the experimental results.

2.1   Wall configurations

The analysed wall configurations stem from two experimental studies on the same masonry typology: walls made of vertically perforated clay blocks with normal thickness bed-joints and normal strength mortar. All tests are quasi-static cyclic shear-compression tests in which the axial load was kept constant and the wall was subjected to cycles of horizontal drifts of increasing amplitude. From each experimental study, two walls are analysed, which have identical dimensions but are subjected to different static boundary conditions. They were chosen to cover various types of failure modes. The two walls of the first study, T1 and T3 [13], fail due to diagonal shear cracking. They were both subjected to double-bending but differed with regard to the applied axial load. The walls of the second study are PUP3 and PUP4 [14], which developed a flexure controlled behaviour including rocking and toe crushing. The two walls differed again with regard to the axial load ratio. Both walls were tested applying a constant shear span of 1.5 times the wall height.

Table 1: Walls simulated to validate the numerical model.

Name/no.	Reference	L [mm]	H [mm]	h_B [mm]	l_B [mm]	σ_0 [MPa]	f_u [Mpa]	$f_{B,c}$ [Mpa]	H_0/H [-]	σ_0/f_u [%]
T1	[13]	2700	2600	190	290	0.58	5.80	26.3	0.5	10
T3	[13]	2700	2600	190	290	1.16	5.80	26.3	0.5	20
PUP3	[14]	2010	2250	190	300	1.05	5.86	35.0	1.5	18
PUP4	[14]	2010	2250	190	300	1.54	5.86	35.0	1.5	26

L: wall length, H: wall height, l_B: brick length, h_B: brick height, σ_0: axial stress applied at the beginning of the test, f_u: compressive strength of masonry, $f_{B,c}$: compressive strength of brick, H_0 / H: shear span-to-wall height ratio, σ_0/f_u: axial load ratio

2.2   Numerical model

The masonry walls are simulated in Abaqus 6.14 [24] using the modelling approach and a material subroutine developed by Aref and Dolatshahi [25]. The simulation is conducted as a dynamic analysis with an explicit solution method.

2.2.1   Modelling approach

The modelling strategy is presented in more detail in [25] and is based on the works of Lourenço [26] and Oliviera et al. [27]. The model is a simplified micro-model in 3D. In this model, the bricks are modelled by solid elements (C3D8R) and the joints as interface elements (COH3D8). Since the interface elements have zero thickness, the bricks are expanded on four sides by half the mortar joint width. The interface elements placed between the bricks represent the bed- and head-joints and will be referred to as horizontal and vertical joints, respectively. Further interface elements (COH3D8) are introduced vertically in the middle of each brick representing a possible fracture plane through the brick. These elements will be referred to as middle joints.

2.2.2   Solid elements

The bricks are modelled as solid elements with a size of $l_{mesh} \sim 7.5$ cm and $h_{mesh} \sim 10$ cm varying slightly between the two chosen walls due to their different brick sizes. The 'Concrete Damaged Plasticity' model, which is available in the material model library of Abaqus, is assigned to the solid elements. The elastic modulus of the brick is estimated based on the brick compressive strength ($E_b = 400\,f_{B,c}$); it differs for the two test campaigns (T1, T3: $E_b=10'520$ MPa, PUP3, PUP4: $E_b=14'000$ MPa) The inelastic stress-strain relationship in compression follows the formulation by Kaushik et al. [28]. In tension, the pre-peak response is linear while the post-peak response follows the exponential law $\sigma_{in} = f_{B,t} \exp(-\varepsilon_{in}\,10^3)$. The compressive brick strength $f_{B,c}$ and the masonry compressive strength f_u had been determined in material tests in both experimental campaigns [13,14] while and the brick tensile strength $f_{B,t}$ was only investigated by [14] and taken as constant for both wall sets as the same masonry typology was used. For the dimensionless parameters of

the concrete damage plasticity model the suggested default parameters for concrete are used [24], which are reproduced in Table 2.

Table 2: Parameters used for the material description of the solid elements in the 'Concrete Damaged Plasticity' model

Series	E_b [MPa]	f_u [MPa]	$f_{B,t}$ [MPa]	v [-]	ψ [deg]	ε [-]	σ_{b0}/σ_{c0} [-]	K_c [-]	μ [-]
T	10'520	5.86	1.27	0.15	31	0.1	1.16	2/3	0
PUP	14'000	5.80							

Nomenclature following [24]; Eb: elastic modulus brick, f_u: compressive strength masonry, $f_{B,t}$: tensile strength brick, v: Poisson's ratio, ψ: dilation angle for flow potential equation, ε: eccentricity, parameter in flow potential equation, σ_{b0}/σ_{c0}: ratio of initial equibiaxial compressive yield stress to initial uniaxial compressive yield stress, K_c: constant in function describing yield surface, μ: viscosity parameter representing relaxation time of viscoplastic system in viscoplastic strain rate tensor

To account for a confinement effect at the wall base, which leads to higher compressive strengths of masonry in the first row of bricks as has been shown in tests by e.g. [29], the first brick row for the flexure controlled walls (PUP3 and PUP4, of which the failure mode is governed by toe crushing at the wall base) are assigned twice the masonry compressive strength f_u. In the absence of a better method to quantify the confinement effect at the walls base, this approach has already been chosen in analytical modelling of the force-displacement behaviour of URM walls by [30,31] and was found to yield good estimates of force and drift capacities.

2.2.3 Interface elements

The behavior of the interface elements is described by a user-defined VUMAT subroutine developed by Aref and Dolatshahi [25]. The subroutine describes the joint behaviour based on a plasticity model featuring an exponentially degrading yield surface in tension and shear. The slope of degradation is defined by the respective fracture energies (tension: G_f^I, shear: G_f^{II}). The model accounts for a straight tension cut-off (at the tensile strength f_t) and a Mohr-Coulomb friction law with friction coefficient $\tan \Phi$ and cohesion c. The cyclic degradation of the elastic normal (k_n) and shear ($k_{sx,y}$) stiffness of the joints is based on plastic multipliers and a degradation parameter (κ_1/κ_t) [32]. The degradation of the shear stiffness $k_{sx,y}$ is limited to 20 % of its initial value, which was found to capture the stiffness of the final cycles rather accurately. The normal stiffness k_n is only reduced in tension while it is set to its initial value upon compressive re-loading to properly simulate the opening and closing of horizontal flexural cracks in bed-joints [25]. The chosen material and degradation parameters are listed in Table 3 with the origin of the parameters being summarised in Table 4.

Table 3: Parameters used to model the joints

Parameter	Unit	T-series			PUP-series		
		Hor. joint	Vert. joint	Mid. joint	Hor. joint	Vert. joint	Mid. joint
f_t	[MPa]	0.14	0.04	1.27	0.14	0.04	1.27
G_f^I	[J/m²]	125	34	107	125	33	107
c	[MPa]	0.26	0.07	1.91	0.27	0.07	1.91
$\tan \Phi$	[-]	0.94	0.94	0.75	0.94	0.94	0.75
G_f^{II}	[J/m²]	1250	339	1068	1250	326	1068
k_n	[N/mm³]	28.9	7.81	400	25.4	11.1	400
$k_{sx,y}$	[N/mm³]	5.93	1.62	400	5.54	2.44	400
κ_1/κ_t	[-]	0.76	0.76	0.76	0.76	0.76	0.76

With the nomenclature according to [25]; f_t: tensile strength, G_f^I: tensile softening energy, c: cohesion, $\tan \Phi$: friction coefficient, G_f^{II}: shear softening energy, k_n: normal stiffness of joints, $k_{sx,y}$: transverse stiffness of joints, κ_1/κ_t: stiffness degradation factor

Table 4: Origin of parameters used to model the joints

Parameter	T-series			PUP-series		
	Hor. joint	Vert. joint	Mid. joint	Hor. joint	Vert. joint	Mid. joint
f_t	Eq. (1)	$f_{t,hor}/4$	Test [14]	Eq. (1)	$f_{t,hor}/4$	Test [14]
G_f^I	assumed	Eq. (7)	Eq. (8)	assumed	Eq. (7)	Eq. (8)
c	Test [13]	Eq. (1)	Eq. (1)	Test [14]	Eq. (1)	Eq. (1)
$\tan \Phi$	Test [14]	Test [14]	assumed	Test [14]	Test [14]	assumed
G_f^{II}	10 G_f^I	10 G_f^I	10 G_f^I	10 G_f^I	10 G_f^I	10 G_f^I
k_n	Eq. (2)	Eq. (2)	very high	Eq. (2)	Eq. (2)	very high
$k_{sx,y}$	Eq. (4)	Eq. (4)	very high	Eq. (4)	Eq. (4)	very high
κ_1/κ_t	[32]	[32]	[32]	[32]	[32]	[32]

Assuming a bi-linear approximation of a parabolic initial yield surface in the tension-shear domain, the tensile strength (f_t) can be given based on the cohesion (c) and the friction coefficient ($\tan\Phi$):

$$f_t = \frac{c}{2\tan\phi} \tag{1}$$

The equivalent elastic normal stiffness of a zero-thickness interface element representing a wall bed-joint (horizontal joint) can be determined from the elastic modulus of the mortar (E_m) and the brick (E_b) as well as the thickness of a mortar joint (h_m) (as presented in e.g. [26]):

$$k_n = \frac{1}{h_m} \frac{E_m E_b}{E_b - E_m} \tag{2}$$

The elastic modulus of the mortar can be back-calculated from the brick elastic modulus and the Young's modulus of the composite material masonry (E_{mas}), which is often determined in tests, using:

$$E_m = \frac{H_m}{\dfrac{H_b + H_m}{E_{mas}} - \dfrac{H_b}{E_b}} \tag{3}$$

where H_m is the combined mortar joint thickness and H_b denotes the sum of brick heights along the wall height. Similar to Eq. (2), the equivalent elastic shear stiffness of a zero-thickness interface element representing a wall bed-joint can be obtained from the mortar (G_m) and the brick (G_b) shear moduli:

$$k_{sx,y} = \frac{1}{h_m} \frac{G_m G_b}{G_b - G_m} \tag{4}$$

The mortar shear modulus can, parallel to Eq. (3), be back-calculated from the shear modulus of the masonry (G_{mas}) and the shear modulus of the brick:

$$G_m = \frac{H_m}{\dfrac{H_b + H_m}{G_{mas}} - \dfrac{H_b}{G_b}} \tag{5}$$

The brick shear modulus can approximately be obtained using elasticity theory:

$$G_b = \frac{E_b}{2(1 + v)} \tag{6}$$

with v being the Poisson's ratio of the brick (see Table 2). The shear modulus of the composite material masonry is estimated according to [30] based on the elastic modulus using $G_{mas} = 0.25 \, E_{mas}$, as the provisions in Eurocode 6 Part 1 [33] and FEMA 356 [3], $G_{mas} = 0.40 \, E_{mas}$, seem to be too high for structural elements in masonry, e.g. [34].

The stiffness of the interface elements representing the head-joints (vertical joints) can be obtained corresponding to Eq. (2) and (4) with the elastic modulus and the shear modulus of the mortar assumed to be one third of the moduli used in the computation of the stiffnesses of the horizontal joints. The stiffnesses of the middle joints representing possible crack planes in the bricks are set to a very high value (around one order of magnitude higher than the stiffness of vertical and horizontal joints) to minimize any influence on the brick stiffness until cracking of the brick starts. It, however, shall not be chosen as too high a value, for the highest

8

stiffness in the system plays a role in determining the time step used in the explicit dynamic analysis—the higher the stiffness, the smaller the time step, the longer is the analysis.

The fracture energy in tension for the vertical joints is assumed to be proportional to the fracture energy of mode I of the horizontal joints times the ratio of the horizontal and vertical joints' tensile strengths:

$$G_{f,vert}^{I} = G_{f,hor}^{I} \frac{f_{t,vert}}{f_{t,hor}} \tag{7}$$

The mode I fracture energy of the middle joints is obtained integrating the inelastic tensile law assigned to the bricks on the stress-displacement level.

$$G_{f,mid}^{I} = \int_{0}^{w_{max}} \sigma_{in}(w)dw \tag{8}$$

with the displacements (w) being the inelastic strains (ε_{in}) times a characteristic length of around 7.5 cm based on the mesh size.

2.3   Validation of the model

The numerical model is validated simulating T1, T3, PUP3 and PUP4 applying the loading protocol used in the respective tests and comparing numerical to experimental results. Figure 2 shows the shear force-drift curves from the individual tests and the corresponding numerical simulation. Figure 3 includes photos of the physical walls at failure. Furthermore the equivalent plastic strain distribution in the solid elements is presented. Equivalent plastic strains (ε_{peeq}) in Abaqus [13] are a scalar measure computed from the plastic strain components (ε_{pl}) using $\dot{\varepsilon}_{peeq} = (2/3\ \dot{\varepsilon}_{pl} : \dot{\varepsilon}_{pl})^{1/2}$ for classical van Mises plasticity. Within the concrete damaged plasticity model, it represents the equivalent plastic strain in uni-axial compression, i.e. it is a measure of how far the current stress-strain state in the element has progressed along the assigned in-elastic uni-axial stress-strain law in compression and is defined as: $\int \dot{\varepsilon}_{peeq}\ dt$. As such it is a good measure of brick crushing. In addition, the deformed shapes of the simulated walls near ultimate drift are provided as well.

For all four walls, the numerically simulated force-displacement response matches the experimental one rather well and also the equivalent plastic strains roughly match the real brick damage patterns. From the deformed shapes it can be seen that bed-joint sliding and uplift in the bed-joints seem to be well captured by the

subroutine. This applies for all observed failure modes, i.e., bed-joint sliding, diagonal cracking and damage within the whole wall area for shear dominated walls (Figure 3a, b) and rocking along with a concentration of damage at the wall toe in the flexure controlled walls (Figure 3c, d).
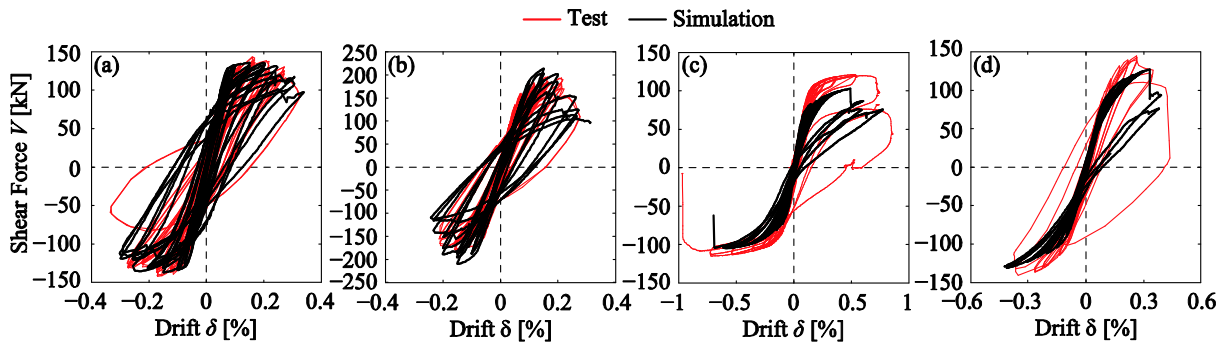

Figure 2: Shear force-drift curves of tests and numerical analysis, (a) T1 by [13], (b) T3 by [13], (c) PUP3 by [14], (d) PUP4 by [14]
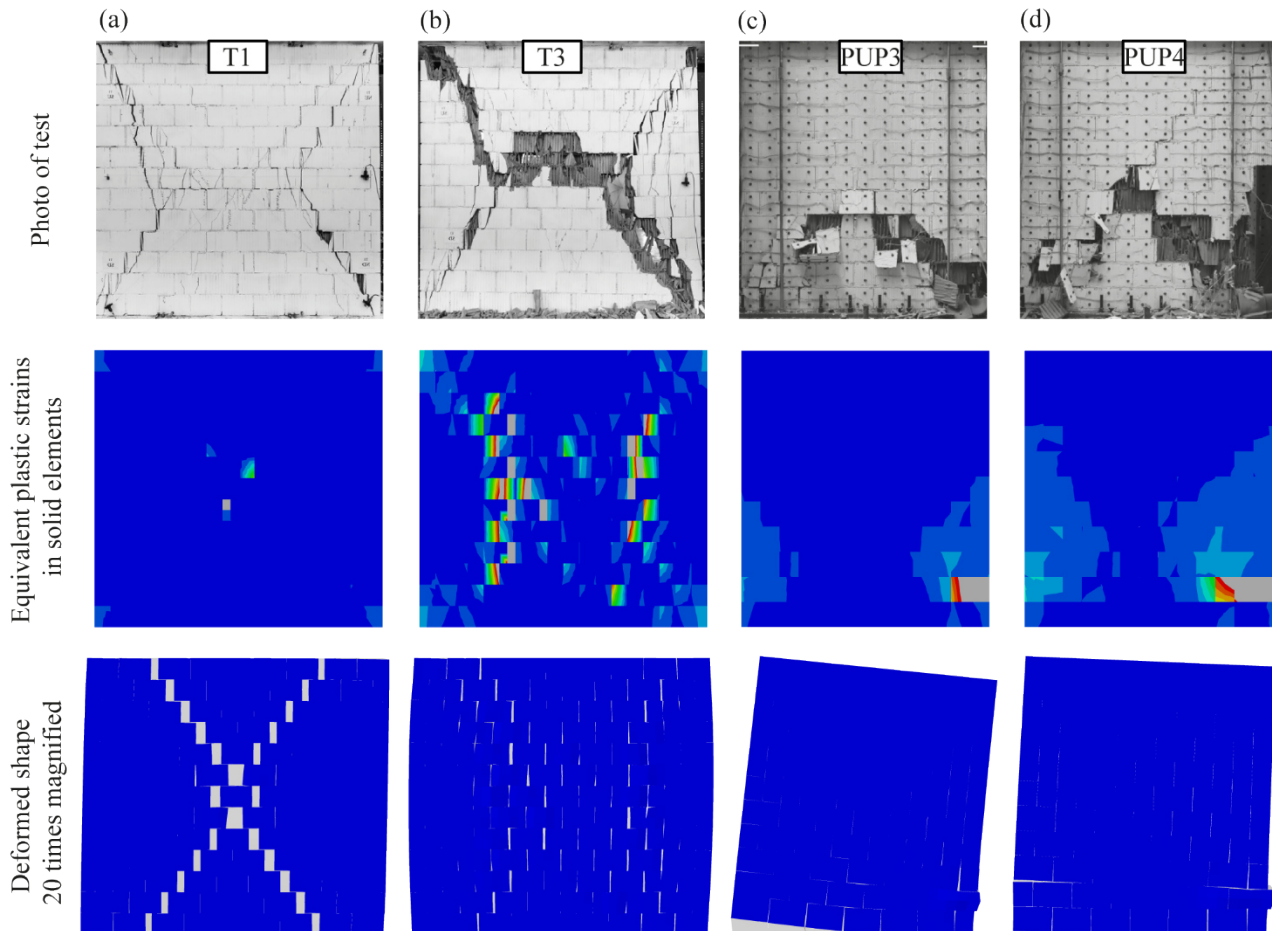

Figure 3: Top row: photos of test specimens at failure, middle row: plastic equivalent strains in solid elements near ultimate drift, bottom row: deformed shapes (20 times magnified) near ultimate drift for (a) T1 by [13], (b) T3 by [13], (c) PUP3 by [14], (d) PUP4 by [14]

Table 5 provides a quantitative comparison between simulations and tests. It compares the results with regard to the peak shear capacity V_{Peak}, the effective stiffness and the ultimate drift. The effective stiffness is the stiffness of the wall when first attaining 0.7 V_{Peak} and the ultimate drift is defined as the drift in the post-peak range at which the shear force of the envelope response drops for the first time below 0.8 V_{Peak}. For all three quantities, the mean ratio of simulation to test result is approximately 0.90 and the standard deviation 0.15.

Table 5: Validation of numerical model by means of comparison to test results of peak shear capacity, effective stiffness and ultimate drift

Wall	V_{Peak} [kN]			k_{ef} [kN/mm]			δ_{ult} [%]		
Name	Sim	Test	S/T	Sim	Test	S/T	Sim	Test	S/T
T1	137	144	0.95	75	73	1.03	0.31	0.28	1.11
T3	213	197	1.08	76	107	0.71	0.20	0.22	0.91
PUP3	102	118	0.86	34	38	0.89	0.50	0.70	0.71
PUP4	127	143	0.89	38	46	0.83	0.33	0.36	0.92
Mean			0.95			0.86			0.91
Std			0.10			0.13			0.16

3   Parametric study

To investigate the influence of the loading history on effective stiffness, strength and drift capacity of URM walls, a series of wall configurations (Section 3.1) is subjected to a number of loading protocols (Section 3.2).

3.1   Wall configurations analysed in the parametric study

The wall configurations analysed in the parametric study correspond to the wall tests against which the numerical model was validated (Section 2.1). As the analysis of the shear dominated walls (T1 and T3) showed a significant dependency of wall capacities on the loading protocol (Section 4), the wall configuration of the first test series are analysed for various axial load ratios and shear spans. All considered wall configurations are listed in Table 6.

Table 6: Walls simulated in the parametric study. Walls in bold are configurations that have been tested experimentally.

Name/no.	Reference	L [mm]	H [mm]	h_B [mm]	l_B [mm]	σ_0 [MPa]	f_u [Mpa]	$f_{B,c}$ [Mpa]	H_0/H [-]	σ_0/f_u [%]
T1	[13]	**2700**	**2600**	**190**	**290**	**0.58**	**5.80**	**26.3**	**0.5**	**10**
2	-	2700	2600	190	290	0.58	5.80	26.3	1.0	10
3	-	2700	2600	190	290	0.87	5.80	26.3	0.5	15
4	-	2700	2600	190	290	0.87	5.80	26.3	1.0	15

		L	H	l_B	h_B	σ_0	f_u	$f_{B,c}$	H_0/H	σ_0/f_u
T3	[13]	**2700**	**2600**	**190**	**290**	**1.16**	**5.80**	**26.3**	**0.5**	**20**
6	-	2700	2600	190	290	1.16	5.80	26.3	1.0	20
7	-	2700	2600	190	290	1.45	5.80	26.3	0.5	25
8	-	2700	2600	190	290	1.45	5.80	26.3	1.0	25
9	-	2700	2600	190	290	1.74	5.80	26.3	0.5	30
10	-	2700	2600	190	290	1.74	5.80	26.3	1.0	30
PUP3	[14]	**2010**	**2250**	**190**	**300**	**1.05**	**5.86**	**35.0**	**1.5**	**18**
PUP4	[14]	**2010**	**2250**	**190**	**300**	**1.54**	**5.86**	**35.0**	**1.5**	**26**

L: wall length, *H*: wall height, l_B: brick length, h_B: brick height, σ_0: axial stress applied at the beginning of the test, f_u: compressive strength of masonry, $f_{B,c}$: compressive strength of brick, H_0 / H: shear span-to-wall height ratio, σ_0/f_u: axial load ratio

3.2   Loading protocols for the parametric study

A widely used loading protocol for quasi-static cyclic tests is the protocol defined by FEMA 461 [22]. It has been proposed for tests on structural and non-structural members without further specifying the material or member type and all other loading protocol variations will be based on it. The protocol consists of a series of zero-mean drift cycles with increasing amplitudes. FEMA 461 recommends to apply two cycles ($n_1 = 2$) per drift limit δ_i and more than 10 drift limits before failure ($n \geq 10$). The total number of cycles is therefore n_1 x n. The amplitude is increased following the relation $\delta_{i+1} = 1.4\,\delta_i$. This protocol is defined by the number of cycles per amplitude n_1, the total number of drift limits n, the starting amplitude δ_0 and the maximum drift limit δ_{max}. An example of this loading protocol for $n_1=2$, $n=10$, $\delta_0=0.05\%$ and $\delta_{max}=1\%$ is shown in Figure 4a.

In order to investigate the influence of the parameters that characterize the load history (number of drift limits n, cycles per drift limit n_1, drift limit mean and drift limit sequence) on stiffness, strength and in particular drift capacity of URM walls, the various loading protocols are applied to the wall configurations listed in Table 6. These are the following loading protocols:

i.   Loading protocols as applied in the tests (for the validation of the numerical model, Section 2.3).

ii.   Monotonic excitation.

iii.   Cyclically increasing loading protocol with zero mean cycles according to FEMA 461 [22] (Figure 4a). All of the following variations are based on this protocol.

iv.   Loading protocol as in iii) but with different numbers of cycles (n_1) per drift limit.

v.   Loading protocol as in iii) but with different numbers of drift limits (n).

vi. Loading protocol as in iii) but changing the mean of the cycles ($mean(\delta_i)$) from zero mean as in FEMA 461, via two intermediate means to the non-reversed cyclic case (Figure 4b). The intermediate means are obtained by reducing the drift limits in negative direction to 50% (Figure 4c) and 30% of the corresponding positive ones respectively.

vii. Non-reversed cyclic loading protocols for various numbers of excursions (n_1) per drift limit and various numbers of drift limits (n).

viii. Two random permutations of the reference loading protocol iii) (Figure 4d) to investigate a possible influence of the drift limit sequence.
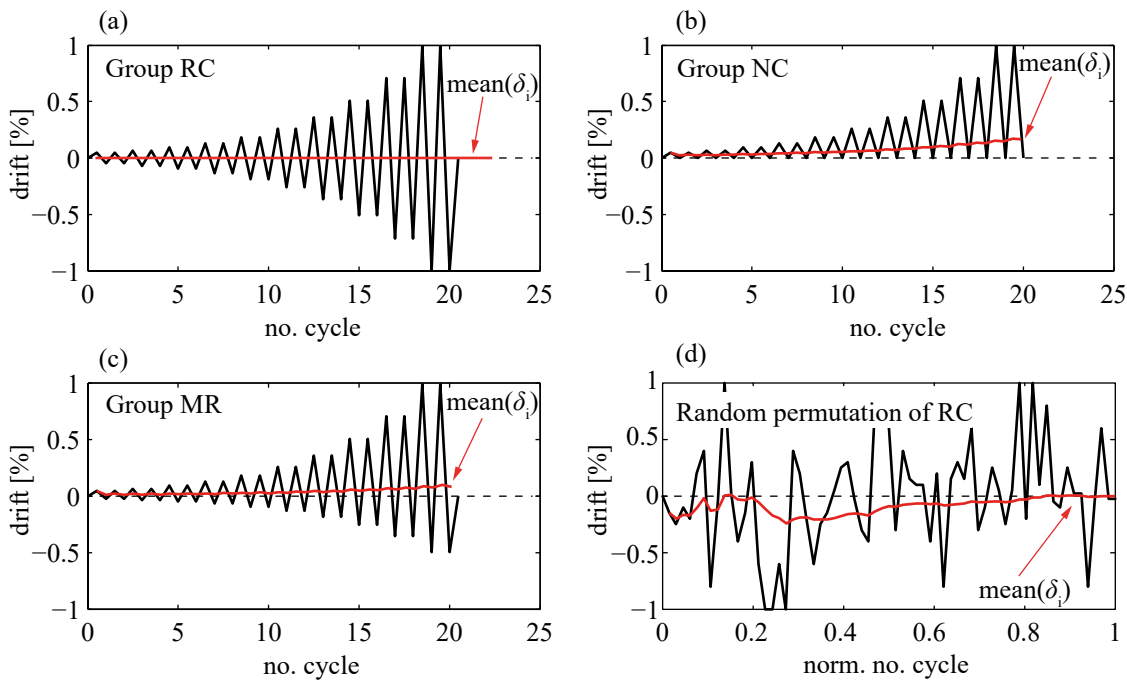
Figure 4: Different loading protocols to be used in the study, up to a drift limit of 1 % with drift limits according to FEMA 461 [22]: (a) reversed-cyclic with n_1=2, (b) non-reversed-cyclic, n_1=2, (c) reversed-cyclic, n_1=3, (c) non-zero mean, reversed-cyclic, n_1=2, (d) random permutation of protocol in Figure 4a

The resulting set of loading protocols can be roughly divided into four groups: Monotonic (M), Non-reversed cyclic (NC), reversed-cyclic with a non-zero drift limit mean (MR) and reversed cyclic with a drift limit mean of zero (RC). A summary of all loading protocols to be applied is presented in Table 7.

Table 7: Set of loading protocols used for each of the considered walls

No. for shear walls	No. for flexure walls	Group	Reference δ_i	n [-]	n_1 [-]	mean δ_i [%]
1	1	Monotonic (M)	-	1	1	0.50

13

				n	n_1	mean δ_i
2	-	Non-rev. cyclic (NC)	FEMA 461 [22]	5	2	0.14
3	-	Non-rev. cyclic (NC)	FEMA 461 [22]	7	2	0.16
4	2	Non-rev. cyclic (NC)	FEMA 461 [22]	10	1	0.17
5	-	Non-rev. cyclic (NC)	FEMA 461 [22]	10	2	0.17
6	3	Non-rev. cyclic (NC)	FEMA 461 [22]	10	3	0.17
7	-	Non-zero mean rev. cyclic (MR)	FEMA 461 [22]	5	2	0.13
8	-	Non-zero mean rev. cyclic (MR)	FEMA 461 [22]	7	2	0.08
9	-	Rev. cyclic (RC)	FEMA 461 [22]	10	2	0
10	-	Rev. cyclic (RC)	FEMA 461 [22]	10	2	0
11	4	Rev. cyclic (RC)	FEMA 461 [22]	10	1	0
12	5	Rev. cyclic (RC)	FEMA 461 [22]	10	2	0
13	6	Rev. cyclic (RC)	FEMA 461 [22]	10	3	0
14	-	Rev. cyclic (RC)	Salmanpour et al. [13]	14	3	0
-	7	Rev. cyclic (RC)	Petry & Beyer [14]	12	2	0
15	8	Random permutation	FEMA 461 [22]	10	2	~ 0
16	9	Random permutation	FEMA 461 [22]	10	2	~ 0

n ... number of drift limits up to a reference drift of 1 %, n_1 … cycles per drift limit, mean δ_i calculated up to reference drift of 1 %

4 Results of the parametric study

The influence of the load history on the effective stiffness k_{ef}, the peak shear strength V_{Peak}, the ultimate drift capacity δ_{ult}, the drift at peak shear strength δ_{Peak} and on the dissipated energy ε_d is investigated in the following. The dissipated energy is defined as the area of the force-displacement hysteresis loops up to the point of ultimate drift.

4.1 Shear controlled walls

Figure 5, which shows the envelope curves of all simulations based on the specimens T1 and T3 [13], highlights that the ultimate drift capacities δ_{ult}, which are indicated with vertical dashed lines for each simulation, vary rather strongly between the various loading protocols. The effective stiffness and the force capacity are significantly less sensitive to the applied loading protocol. For most wall configurations, monotonic loading leads to around double the ultimate drift capacity than reversed-cyclic loading protocols. This agrees with the experimental findings by e.g. Ganz & Thürlimann [5] and Magenes & Calvi [6] (see Section 1). Furthermore, Figure 5 indicates that walls subjected to low axial load ratios and small shear spans are more sensitive to the load history.
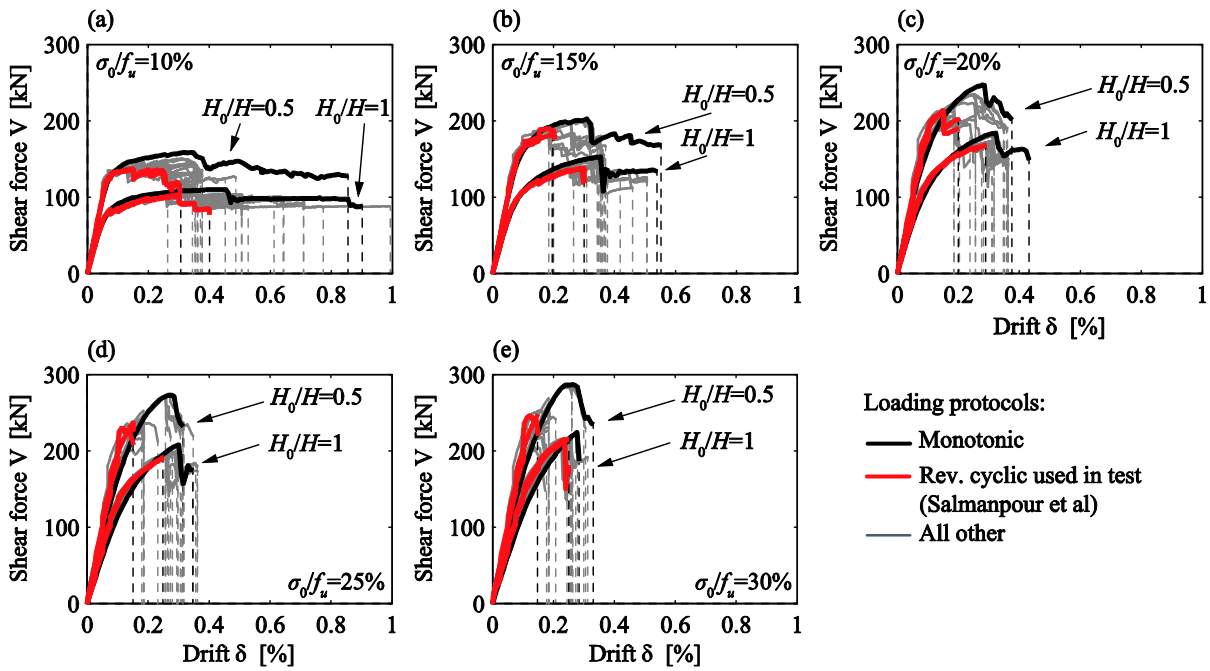
Figure 5: Envelope responses of the simulations for the analysed walls

A more detailed summary of the sensitivity of the characteristic parameters with respect to the load history is presented in Figure 6. For each wall configuration, the values are normalised with regard to the maximum value obtained for all loading protocols. The peak shear capacity (V_{Peak}, Figure 6a) decreases by around 10 % from the monotonic protocol to the reversed-cyclic one. The corresponding drift (δ_{Peak}, Figure 6b), however, decreases rather strongly, in particular for walls with a low axial load ratio and a shear span ratio of 0.5. The effective stiffness (k_{ef}, Figure 6c) varies significantly between non-reversed and reversed cyclic loading and is smaller for the non-reversed cyclic protocols.

The ultimate drift capacity (δ_{ult}, Figure 6d) follows similar trends as the drift at peak force δ_{Peak} but the ultimate drift is in average even more susceptible to the load history than δ_{Peak}. Its sensitivity seems to be particularly strong for walls subjected to a low axial load ratio and a shear span of 0.5. However, also walls with a shear span of one show a clear reduction in ultimate drift capacity, especially for low axial load ratios. It is interesting to see that for low axial load ratios, any non-reversed or reversed cyclic loading protocol leads to a drift capacity that is approximately 50 % lower than the drift capacity obtained with the monotonic protocol. Higher axial load ratios, on the contrary, lead to comparable ultimate drift capacities for monotonic and non-reversed loading protocols and only reversed-cyclic protocols lead to a drop in drift capacity of about 50 %.
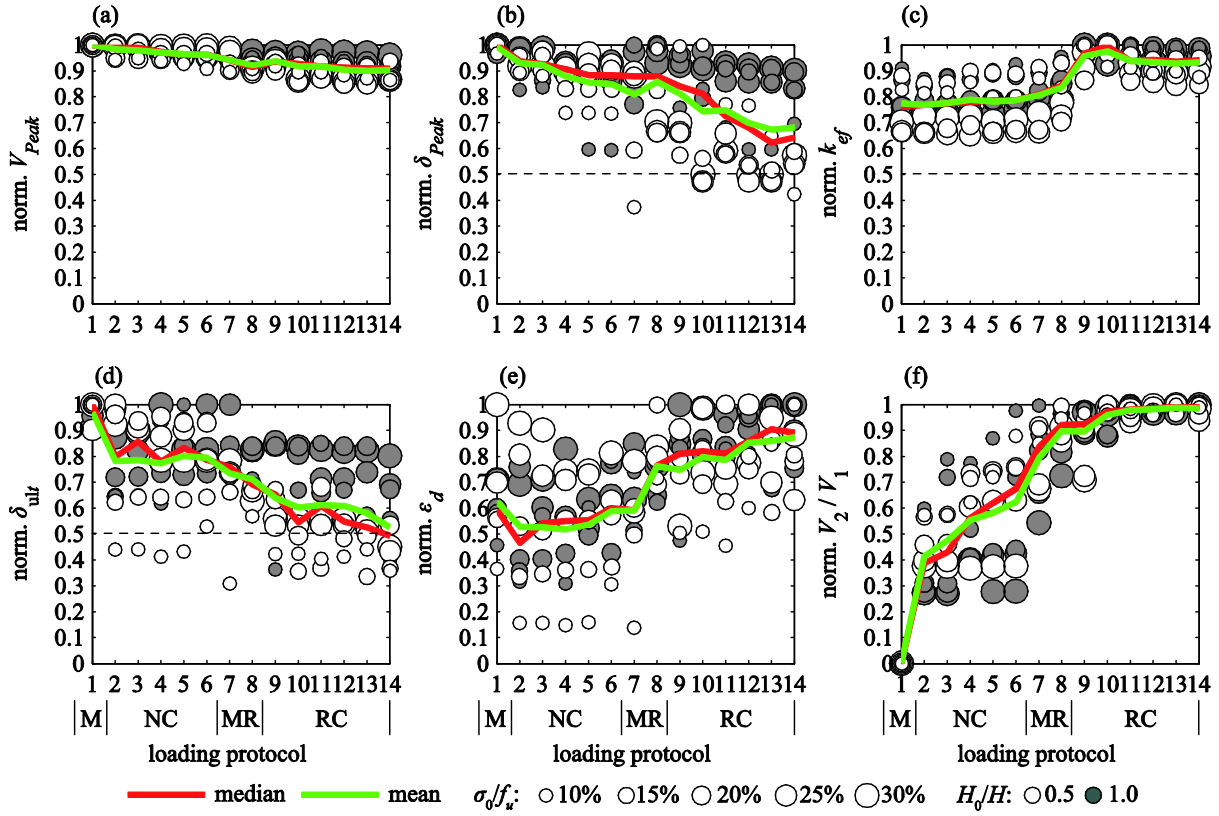
Figure 6: Summary of development of characteristic parameters with applied loading protocols (normalised with respect to the maximum value), (a) peak shear capacity, (b) corresponding drift, (c) effective stiffness, (d) ultimate drift capacity, (e) energy dissipated up to ultimate drift, (f) ratio of maximum shear force in the negative loading direction, V_2, to maximum shear force in the positive loading direction, V_1, up to ultimate drift. Loading protocol groups: M—monotonic, NC—non-rev. cyclic, MR—non-zero mean rev. cyclic, RC—reversed cyclic, zero mean

The dissipated energy ε_d seems to be rather constant for non-reversed (and monotonic) loading protocols but increases considerably for reversed-cyclic ones.

It appears that the drift limit mean, which can be used to characterise the difference between monotonic, non-reversed cyclic and reversed-cyclic loading has a significantly stronger influence on drift capacities and effective stiffness than the number of different drift limits (n) or the cycles per drift limit (n_1). This is illustrated in Figure 7 for sets of loading protocols where only one parameter is changed at a time (only for Figure 7c, more than one parameter changed in the loading protocol selection since it is shown beforehand that the other parameters, n_1 and n, do not play a significant role as described in the following). While the mean and median of the ultimate drift capacities do not show a significant trend with the number of drift limits n (Figure 7a) and the cycles per drift limit n_1 (Figure 7b), it clearly shows a positive trend for the mean of the drift limits (Figure 7c). Yet, the simulations with a low axial load ratio of 10 % and a shear span ratio of 0.5 seem not to adhere

16

to this trend. This is due to the influence of bed-joint sliding on the symmetry of the damage distribution in the wall, which will be discussed explicitly in Section 4.3.2.
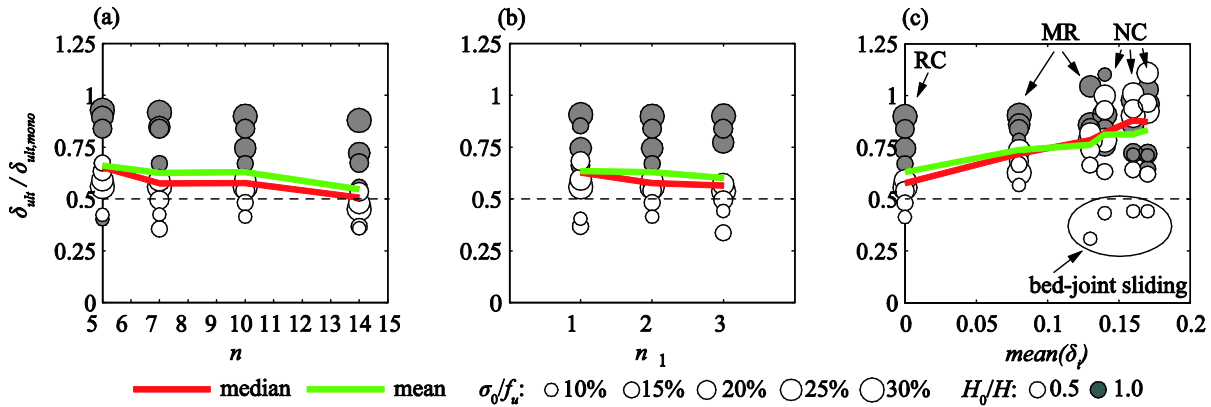

Figure 7: Normalised ultimate drift capacity (with regard to monotonic loading) vs: (a) number of distinct drift limits n, (b) number of excursions per drift limit n_1, (c) mean of the drift limits up to reference drift of 1 %

4.2 Flexure dominated walls

The force-displacement response of flexure dominated walls (Figure 8a) is significantly less sensitive to the load history than for shear controlled walls; as an example the variation of the drift capacity is plotted in Figure 8c. Only the effective stiffness shows a similar sensitivity than for shear controlled walls (Figure 8b).
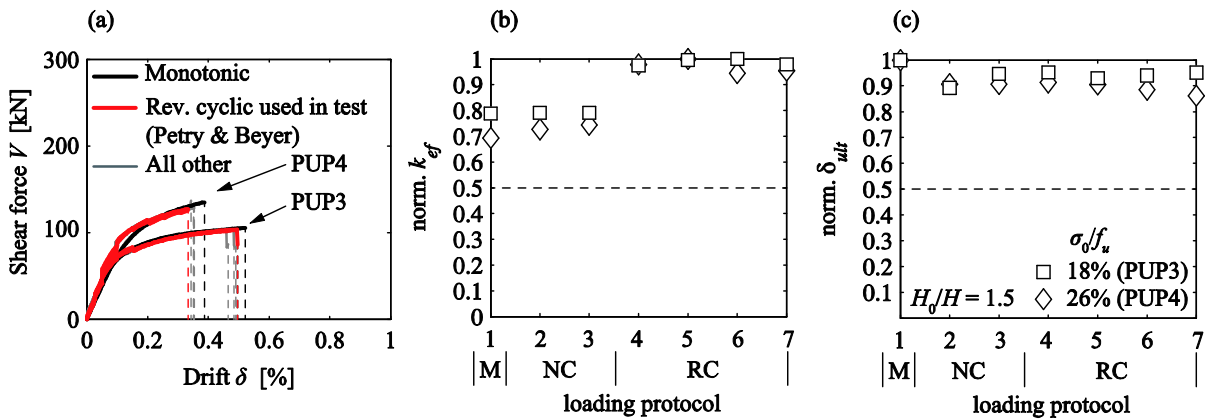

Figure 8: (a) envelops of the simulated force-displacement responses for both walls, change of (b) effective stiffness in considered flexure dominated walls with loading protocols, (c) ultimate drift capacity

4.3 Discussion

4.3.1 Influence of damage localization

Shear controlled walls seem to be more sensitive to the load history than flexure dominated walls. The reason for this difference appears to be the difference in damage distribution within the wall panel. In shear controlled walls with a shear span of 0.5, large parts of the wall are subjected to inelastic deformations in tension (diagonal cracks) or compression (brick crushing) (see Figure 3a, b). The higher the drift limit mean (skewness of the loading protocol), the lower is the overall damage, e.g. monotonic loading will only damage approximately half of the wall area while reversed-cyclic loading damages the entire wall area and therefore the drift capacity obtained for monotonic loading is higher than the drift capacity obtained for reversed-cyclic loading. In this case, the damages from the two loading directions intersect and damage from one loading direction may also influence the force-displacement behaviour of the wall in the opposite direction of loading. Increasing the shear span-to-wall height ratio from 0.5 to 1.0 leads to a localization of the damage at the wall toe, yet, diagonal cracking still occurs in large parts of the wall so the decrease in ultimate drift with increasing cumulative drift demand is not as pronounced anymore but still clearly discernable. In flexure dominated walls with a shear span of 1.5, however, the damage localizes around the wall toes (as can be seen in Figure 3c, d) whereas the rest of the wall does not experience significant damage. Hence, as soon as crushing occurs in this zone, the wall fails, which significantly reduces its susceptibility to the load history. Furthermore even for the case of reversed-cyclic loading, the localized damaged regions do not intersect and seem not to significantly influence the force-displacement behavior of the wall in the opposite loading direction.

4.3.2 Influence of bed-joint sliding

The drop in drift capacities in walls with a low axial load ratio as soon as any cyclic loading protocol is applied can be attributed to bed-joint sliding. For high axial load ratios, sliding is not a dominant deformation mode. Significant sliding leads to a more immediate decrease in drift capacity since it causes large plastic drifts that need to be overcome when unloading and reloading in the other direction. Already unloading to zero drift introduces therefore rather high shear loads and hence cracking and crushing in the second loading direction. This results even for non-reversed cyclic loading protocols in a rather symmetric damage distribution

throughout the wall. Figure 6f shows the normalized ratio of maximum shear force in the negative loading direction to the maximum shear force in the positive direction (V_2 / V_1) for the various applied loading protocols. While walls with higher axial load ratios show generally moderate shear force ratios (V_2 / V_1) of below 0.5 for non-reversed loading protocols, walls with a low axial load ratio have significantly higher shear force ratios. For high axial load ratios a strong reduction in drift capacity is therefore only observed for reversed-cyclic protocols, while for low axial load ratios such a reduction is also observed for non-reversed cyclic loading protocols.

4.3.3 Difference in effective stiffness

The analysis indicates a difference in effective stiffness between non-reversed and reversed-cyclic loading protocols, with the effective stiffness for the latter being up to 50 % higher (see Figure 6c). This can be attributed to the very definition of the effective stiffness, which, as outlined previously, is computed herein as the stiffness of the envelope response at first attainment of 0.7 times the peak shear capacity. Yet, this takes typically place when the wall is already damaged and, hence, the cyclic force-displacement response features a residual drift. Upon re-loading, in the reversed-cyclic case, this residual drift leads to a higher load level than in the previous cycle. This is visualized in Figure 9a. Thus, the wall appears stiffer than for a monotonic or non-reversed-cyclic protocol where this load level is only reached at a higher drift since no negative residual drift has to be overcome.
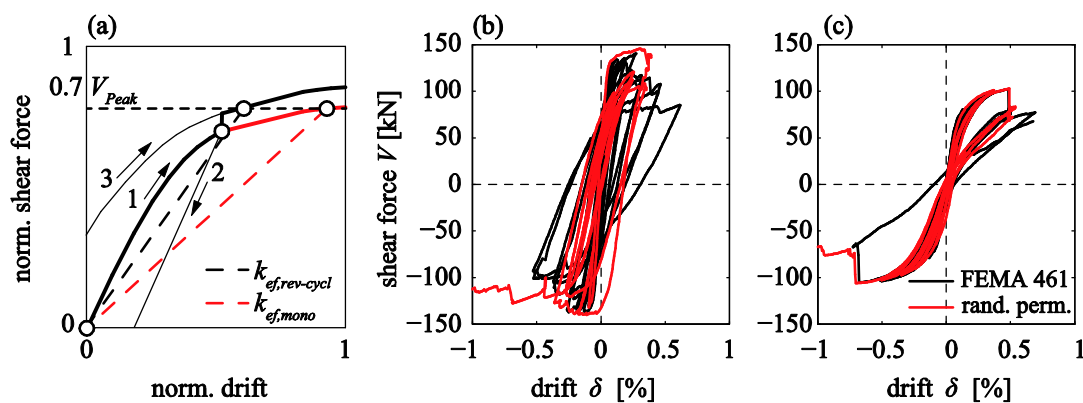

Figure 9: (a) representation of reason for difference in effective stiffness between reversed-cyclic and non-reversed loading, shear force-displacement curves showing simulation of cyclic loading protocol according to FEMA 461 [22] and random permutation of it for (b) wall T1 [13], (c) wall PUP3 [14]

4.3.4 Sequence of drift amplitudes

The influence of the order of drift amplitudes was investigated by means of applying random permutations of the reversed-cyclically increasing reference loading protocol according to FEMA 461 [22]. Figure 9b and c show representative examples of force-displacement curves of a shear controlled wall (T1) and a flexure controlled wall (PUP3) subjected to a random permutation of the FEMA 461 loading protocol. While the behaviour of the shear controlled wall is sensitive to the sequence of drift amplitudes, this does not apply to the flexure controlled wall. This supports the finding that flexure controlled walls are not very susceptible to a change in load history while shear walls are. For a random permutation of the FEMA 461 loading protocol higher shear force and drift capacities in the shear controlled wall are obtained than the original reversed-cyclically increasing FEMA 461 protocol. Changing the order of drift limits in shear controlled walls by means of a random permutation can lead to a less symmetric damage distribution throughout the wall and, thus, a higher force and drift capacity. Hence, this loading condition will lead to force and displacement capacities in-between monotonic and reversed-cyclic loading depending on the position of the largest amplitudes within the entire loading protocol (e.g. largest amplitude first corresponds to monotonic loading, increasing drifts with largest amplitude last corresponds to reversed-cyclic loading). Therefore, using a reversed-cyclically increasing protocol, i.e., protocols such as in FEMA 461, the smallest values for strength and displacement capacity are obtained.

4.3.5 Limitations of approach

The results of this study are based on 160 numerical simulations of various wall configurations. This approach has of course some limitations. First, the observed trends strictly apply only for an H / L ratio of around one—the wall aspect ratio of the simulated walls. It was demonstrated in the previous section that the effect of the load history on stiffness, strength and drift capacity depends mainly on the damage pattern, which might change for different wall aspect ratios. Second, the study was limited to one masonry typology, i.e., walls with vertically perforated clay units and bed-joints of normal thickness with normal strength mortar. The numerical study should, therefore, be regarded as a research approach that yields first insights into the effect of the load history on the wall performance. For the future, it is recommended to validate the identified trends through an

extensive experimental campaign that investigates explicitly the influence of the load history on the force, stiffness and drift capacities of URM walls.

5 Correlation between ultimate drift capacity and load history

This section introduces a simple empirical model that links the drift capacity to the applied loading protocol. It solely applies to shear controlled walls, because flexural walls were found to be insensitive to the load history (see Section 4.2). As can be seen in Figure 10a, the cumulative drift demand does not correlate well with the drift capacity. The analyses showed that the decrease in drift capacity for shear controlled walls seems to be related to two main factors. The first factor is the axial load ratio, which can be seen as a measure for the extent to which bed-joint sliding contributes to the wall deformations. Figure 10b shows that the lower the axial load ratio, the higher is the scatter of ultimate drift capacities. The second factor appears to be the mean of the single drift limits, which can be seen as a measure of the symmetry of loading and, hence, the damage in the wall, e.g. a mean of zero (symmetric reversed-cyclic loading) leads to the most widely spread damage throughout the wall resulting in a maximum decrease of drift capacity compared to the drift capacity under monotonic loading, which only results in roughly half the damage.
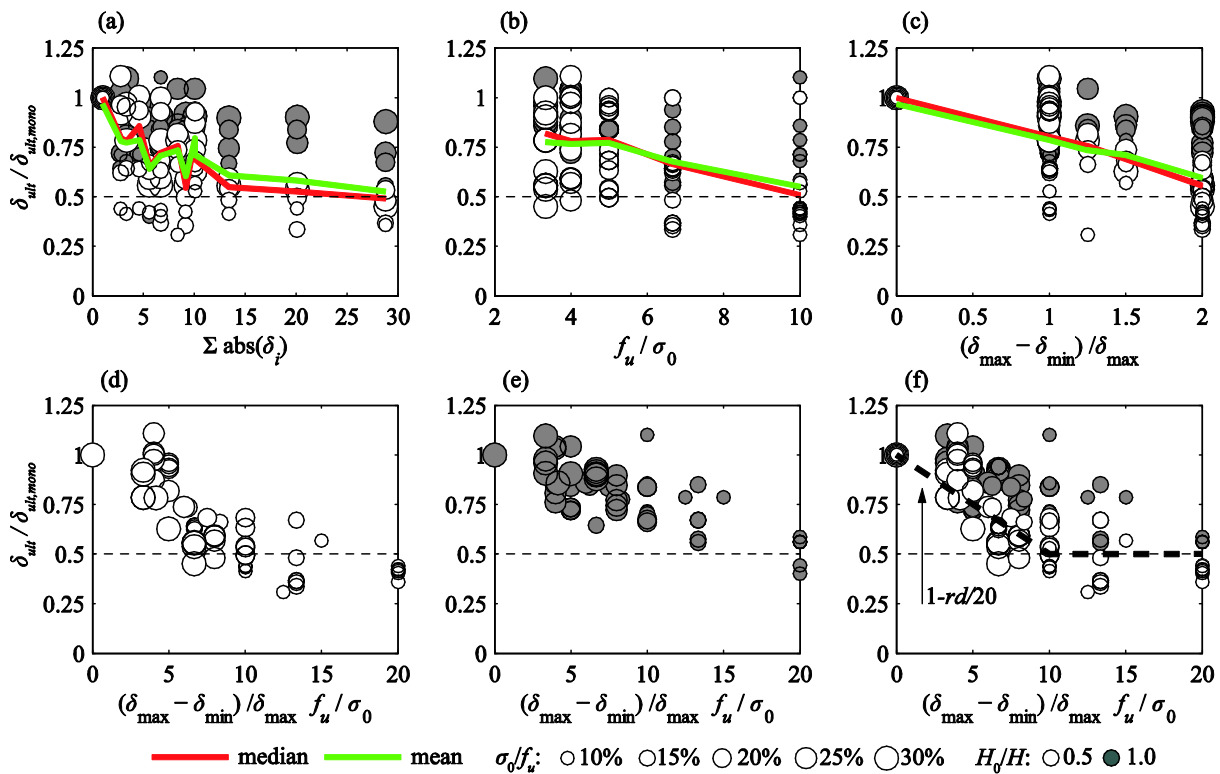
Figure 10: Normalised ultimate drift capacities (with respect to monotonic loading) vs (a) sum of drift limits, (b) inverse of axial load ratio, (c) 'skewness' of loading protocol, (d) representative demand—walls with shear span ratio of 0.5, (e) representative demand—walls with shear span ratio of one, (f) representative demand—all walls'

Based on these observations, the following *representative demand (rd)* measure is proposed:

$$rd = \frac{\delta_{max} - \delta_{min}}{\delta_{max}} \frac{f_u}{\sigma_0} \tag{9}$$

The first term of Eq. (9) is a measure of the skewness of the load history. It is zero for a monotonic, one for a non-reversed cyclic and two for a reversed cyclic loading protocol. Figure 10c shows the normalized drift capacities vs this first factor. The second part of Eq. (9) is the inverse of the axial load ratio and accounts for the influence of bed-joint sliding. As can be seen in Figure 10d and e, the measure of the representative demand correlates well with the decrease in ultimate drift capacity and can therefore be used to estimate the drift capacity under any load history from the drift capacity under reversed cyclic loading with cycles of zero mean (i.e., the most commonly applied loading protocols such as FEMA 461). It is suggested to approximate the correlation function by the following bilinear relationship (Figure 10f):

$$\delta_{ult}(rd) = \begin{cases} \delta_{ult,mono}\left(1 - \dfrac{rd}{20}\right) & \text{for } 0 \le rd < 10 \\ 0.5\ \delta_{ult,mono} & \text{for } rd \ge 10 \end{cases} \tag{10}$$

With the lower bound estimate of:

$$\delta_{ult,mono} \sim 2\delta_{ult,rev-cyc} \tag{11}$$

the ultimate drift capacity $\delta_{ult}(rd)$ can be based on the ultimate drift capacity of walls under reversed-cyclic loading with a non-zero drift limit mean $\delta_{ult,rev-cyc}$, which will be most commonly known from test results.

$$\delta_{ult}(rd) \cong \begin{cases} 2\delta_{ult,rev-cyc}\left(1 - \dfrac{rd}{20}\right) & \text{for } 0 \le rd < 10 \\ \delta_{ult,rev-cyc} & \text{for } rd \ge 10 \end{cases} \tag{12}$$

6   Conclusions

This article treats the influence of the load history on the force-displacement response of in-plane loaded URM walls by means of a numerical study. One main finding of this study is that the load history has a significant

influence on the drift capacity of shear controlled walls but only a negligible influence on the drift capacity of flexure dominated walls. The effective stiffness and shear strength of shear controlled walls are less affected by the load history than the drift capacity.

It was found that the key difference between shear and flexure controlled walls is the spread of damage over the wall panel. The wider the damage is spread, the more sensitive is the wall to the load history since the damage that occurs when loading in one direction also affects the response when loading in the opposite direction. Shear controlled walls are characterized by diagonal cracking, which affects the entire wall area. Hence, such walls show a rather strong dependency of the ultimate drift on the applied load history. For reversed-cyclic loading, the ultimate drift capacity is only about half the drift capacity obtained for monotonic loading, which confirms experimental findings [5,6]. Flexure dominated walls, on the contrary, which are characterized by rocking with localized toe crushing at failure, hardly show any sensitivity of the drift demand to the applied load history. The more localized the damage, the smaller is the wall's susceptibility to the load history. Walls of any behaviour type displayed a slightly smaller shear force capacity and a slightly larger effective stiffness for cyclic than for monotonic loading.

It appears, that the number of excursions per drift limit and the number of different drift limits do not have a significant influence on the five characteristic wall parameters that were investigated (k_{ef}, V_{peak}, δ_{peak}, δ_{ult} and ε_p) but the mean of the cycles is the most influential parameter. Symmetric reversed-cyclic loading protocols with a zero mean cause the most wide-spread damage in shear controlled walls and therefore lead to the smallest drift and force capacities. However, in particular for walls subjected to high axial load ratios, where sliding deformations play only a subordinate role, not all cyclic loading protocols lead to similar drift capacities. Such walls support higher drifts if they are loaded in a non-reversed manner, which might occur in real earthquake conditions due to the ratcheting effect [9]. Based on these results, an expression was proposed that allows for estimation of the drift capacity in shear controlled walls as function of the load history, the axial load ratio and the drift capacity for reversed-cyclic loading. Flexure controlled walls are rather insensitive to the load history and monotonic tests might be sufficient to obtain the parameters necessary for seismic design.

This study was based on numerical simulations. Future research should validate the here identified trends through a test campaign that explicitly investigates the influence of the load history on the force, stiffness and

drift capacities of the wall. Based on the results of this study, this experimental study should investigate in particular the sensitivity to the load history for different failure modes and different axial load ratios.

7   Acknowledgement

8   References

[1] CEN. EN 1998-3: 2005 Eurocode 8: Design of structures for earthquake resistance - Part 3: Assessment and retrofitting of buildings. Comité Européen de Normalisation, 2005.

[2] NTC. Decreto Ministeriale 14/1/2008: Norme tecniche per le costruzioni. Ministry of Infrastructures and Transportations, 2008.

[3] ASCE. FEMA 356: Prestandard and Commentary for the Seismic Rehabilitation of Buildings. American Society of Civil Engineers, Reston, Virginia, 2000.

[4] NZSEE. Assessment and Improvement of Unreinforced Masonry Buildings for Earthquake Resistance, New Zealand Society of Earthquake Engineering, supplement to "Assessment and improvement of the structural performance of buildings in earthquakes." University of Auckland, 2011.

[5] Ganz H, Thürlimann B. Versuche an Mauerwerksscheiben unter Normalkraft und Querkraft. Test Report, ETH Zürich: 1984.

[6] Magenes G, Calvi GM. Cyclic behaviour of brick masonry walls. Earthq Eng Tenth World Conf Rotterdam 1992.

[7] Beyer K, Petry S, Tondelli M, Paparo A. Towards Displacement-Based Seismic Design of Modern Unreinforced Masonry Structures. In: Ansal A, editor. Perspect. Eur. Earthq. Eng. Seismol., vol. 34, Cham: Springer International Publishing; 2014, p. 401–28. doi:10.1007/978-3-319-07118-3.

[8] Tomazevic M, Lutman M, Petkovic L. Seismic behavior of masonry walls: experimental simulation. J Struct Eng 1996;122:1040–7.

[9] Krawinkler H. Loading histories for cyclic tests in support of performance assessment of structural components. 3AESE Conf (3rd Int Conf Adv Exp Struct Eng 2009:1–10.

[10] Mergos P, Beyer K. Loading protocols for European regions of low to moderate seismicity. Bull Earthq Eng 2014;504:2507–30. doi:10.1007/s10518-014-9603-3.

[11] Bosiljkov V, Tomazevic M, Lutman M. Optimization of shape of masonry units and technology of construction for earthquake resistant masonry buildings - Part One and Two. Lubljana, Slowenia: 2004.

[12] Bosiljkov V, Tomazevic M, Lutman M. Optimization of shape of masonry units and technology of construction for earthquake resistant masonry buildings - Part Three. Lubljana, Slovenia: 2006.

[13] Salmanpour AH, Mojsilović N, Schwartz J. Displacement capacity of contemporary unreinforced masonry walls: An experimental study. Eng Struct 2015;89:1–16. doi:10.1016/j.engstruct.2015.01.052.

[14] Petry S, Beyer K. Cyclic Test Data of Six Unreinforced Masonry Walls with Different Boundary Conditions. Earthq Spectra 2015;31:2459–84. doi:10.1193/101513EQS269.

[15] ATC. ATC 24: Guidelines for cyclic seismic testing of components of steel structures. Applied Technology Council (ATC), Washington DC, 1992.

[16] Behr R, Belarbi A. Seismic test methods for architectural glazing systems. Earthq Spectra 1996;12. doi:http://dx.doi.org/10.1193/1.1585871.

[17] Clark P, Frank K, Krawinkler H, Shaw R. Protocol for fabrication, inspection, testing and documentation of beam-column connection tests and other experimental specimens. 1997.

[18] Krawinkler H, Parisi F, Ibarra L, Ayoub A, Medina R. Development of a testing protocol for woodframe structures. CUREE, Publication No. W-02: 2001.

[19] CEN. EN 12512 Cyclic testing of joints made with mechanical fasteners. Comité Européen de Normalisation, 2001.

[20] AISC. ANSI/AISC 341-05 Seismic Provisions for Structural Steel Buildings. American Institute of Steel Construction, 2005.

[21] Richards PW, Uang C. Testing Protocol for Short Links in Eccentrically Braced Frames. J Earthq Eng 2006;132:1183–91. doi:http://dx.doi.org/10.1061/(ASCE)0733-9445(2006)132:8(1183).

[22] ATC. FEMA 461: Interim Testing Protocols for Determining the Seismic Performance Characteristics of Structural and Nonstructural Components. Applied Technology Council (ATC), Washington DC, 2007.

[23] Retamales R, Mosqueda G, Filiatrault A, Reinhorn A. Testing Protocol for Experimental Seismic Qualification of Distributed Nonstructural Systems. Earthq Spectra 2011;27:835–56. doi:10.1193/1.3609868.

[24] Dassault Systèmes. Abaqus 6.14 Documentation. Providence, RI, USA: Dassault Systèmes Simulia Corp.; 2014.

[25] Aref AJ, Dolatshahi KM. A three-dimensional cyclic meso-scale numerical procedure for simulation of unreinforced masonry structures. Comput Struct 2013;120:9–23. doi:10.1016/j.compstruc.2013.01.012.

[26] Lourenço PB. Computational strategies for masonry structures. PhD-Thesis, TU Delft, 1996. doi:ISBN 90-407-1221-2.

[27] Oliveira D V., Lourenço PB, Roca P. Cyclic behaviour of stone and brick masonry under uniaxial compressive loading. Mater Struct 2007;39:247–57. doi:10.1617/s11527-005-9050-3.

[28] Kaushik HB, Rai DC, Jain SK. Stress-Strain Characteristics of Clay Brick Masonry under Uniaxial Compression. J Mater Civ Eng 2007;19:728–39. doi:10.1061/(ASCE)0899-1561(2007)19:9(728).

[29] Petry S, Beyer K. Limit states of modern unreinforced clay brick masonry walls subjected to in-plane loading. Bull Earthq Eng 2015;13:1073–95. doi:10.1007/s10518-014-9695-9.

[30] Petry S, Beyer K. Force-displacement response of in-plane-loaded URM walls with a dominating flexural mode. Earthq Eng Struct Dyn 2015;44:2551–73. doi:10.1002/eqe.2597.

[31] Wilding BV, Beyer K. Force–displacement response of in-plane loaded unreinforced brick masonry walls: the Critical Diagonal Crack model. Bull Earthq Eng 2017;15:2201–44. doi:10.1007/s10518-016-0049-7.

[32] Gopalaratnam VS, Shah SP. Softening Response of Plain Concrete in Direct Tension. ACI J 1985;82:310–23. doi:10.14359/10338.

[33] CEN. EN 1996-1-1:2005 Eurocode 6: Design of masonry structures - Part 1-1: General rules for reinforced and unreinforced masonry structures. Comité Européen de Normalisation, 2005.

[34] Tomaževič M. Shear resistance of masonry walls and Eurocode 6: shear versus tensile strength of masonry. Mater Struct 2009;42:889–907. doi:10.1617/s11527-008-9430-6.